Performance of 3D RAMLA with Smooth Basis Functions on Fully 3D PET Data

Samuel Matej, Margaret E. Daube-Witherspoon, and Joel S. Karp

Abstract— **3D reconstructions from fully 3D PET data can yield high-quality images but often at a high computational cost. To obtain practical data processing and reconstruction times, simplified and less precise approaches are used in the routine clinical use. We studied the feasibility of using the 3D row action maximum likelihood algorithm (3D RAMLA) with 3D spherically-symmetric basis functions (blobs) located on an efficient spatial (body centered cubic) grid for clinical PET data. The BCC grid provides more uniform distribution of the basis functions that represent the reconstructed object and decrease the computational time. Another development used in our study is a fast Fourier based forward projector that provides very fast calculation of the attenuation coefficients in fully 3D data space. These two developments move fully 3D reconstruction using appropriate data processing approaches toward clinically practical times. We are studying the practical effects of the use of these more precise approaches to fully 3D reconstruction on clinical data.**

Keywords— **Fully 3D reconstruction, PET, RAMLA, 2.5D reconstruction, smooth basis functions, attenuation correction.**

I. Introduction

MODERN Positron Emission Tomography (PET) scanners are characterized by a large axial Field Of View (FOV) which enables acquisition of data from a large range of oblique angles. Efficient 3D algorithms are needed to process the fully 3D data provided by those scanners in clinically reasonable times. In our previous studies [1–3] on 3D image reconstruction for PET we used various iterative algorithms operating on a series expansion representation of the volume, where the spatial distribution to be reconstructed was represented by the superposition of 3D basis functions [4]. These basis functions, which we call "blobs," are spherically-symmetric with bell-shaped radial profiles. Using a blob basis function inside the reconstruction process preserves the consistent component (true signal) of the data, thus preserving the resolution of the measured data, while at the same time suppressing the stochastic part (noise) of the data, as experimentally confirmed in [1]. Although filtering also suppresses noise, it can not preserve the spatial resolution of the data at the same time. In all of our studies, the 3D iterative reconstructions using blobs provided substantial and consistent improvement over the methods using classical basis functions - voxels. Until recently, the computational demands of the 3D iterative algorithms were found to be too high for routine clinical use.

This work was supported by The Whitaker Foundation and DOE Grant FG02-88ER60642.

Authors are with the Department of Radiology, University of Pennsylvania, 423 Guardian Drive, 4th floor Blockley Hall, Philadelphia, PA 19104, USA (e-mail: matej@mipg.upenn.edu).

To decrease reconstruction times, clinical reconstruction approaches usually involve rebinning of the measured fully 3D data into non-oblique sinogram data within slices, followed by slice by slice reconstruction. The most popular, and clinically used, rebinning technique is Fourier rebinning (FORE) [5]. Rebinning substantially decreases the volume of the data at the expense of reduced quality caused by using 2D reconstruction techniques instead of the 3D methods. In our recent studies [6, 7] we evaluated a 2.5D reconstruction approach (used after FORE) that considerably improves image quality over a pure 2D approach but with computational demands of the same order as those of 2D techniques. The 2.5D reconstruction considerably decreases the computational burden because it uses rebinned data while, at the same time, it takes into consideration volume nature of the measured data (by using 3D blob basis functions) and thus keeps some advantages of the 3D techniques. More precisely, in the 2.5D approach the reconstructions of the individual slices are coupled, and iteration calculations for each projection line are influenced by, and contribute to, several image slices. In our previous studies, images reconstructed by 2.5D algorithms were found to be superior in terms of a number of figures of merit related to resolution and noise to those produced by 2D algorithms, in which the individual slices are handled separately [6, 7]. However, both 2D and 2.5D approaches are affected by rebinning approximation errors as the axial acceptance angle increases [8, 9]. For axial acceptance angles around (or exceeding) $\pm 15°$, as occurs with some of the recent commercial PET scanners, FORE approximation errors already introduce noticeable image artifacts and nonuniform deterioration of axial resolution. There are other more precise rebinning approaches [5], they are, however, computationally more demanding. In addition to the approximation errors, approaches using rebinned data are limited because of the lack of proper reconstruction models taking into account rebinning (and data acquisition) effects.

Image representation using smooth basis functions provides an alternative approach that reduces the computational demands of 3D iterative approaches. This particular image representation allows utilization of a more advantageous spatial grid, compared to the classical voxel (simple cubic) grid. It also leads to a more uniform 3D distribution of the basis functions (grid points) throughout the 3D space, using Body Centered Cubic (BCC) grid based on the effective spatial sampling [10]. This, in turn, allows one to decrease the grid density (number of grid points) without compromising the quality of the image representation. This result has been demonstrated in our previous

studies using simulated data [10] and is reevaluated in this current study using measured PET data.

Proper treatment and utilization of attenuation information plays an important role in whole body PET imaging [11]. For the attenuation information to be treated properly, the attenuation coefficients are needed on the same set of LORs as those of the acquired emission data. In the fully 3D data case, the measured emission data has to be corrected for attenuation before being processed by rebinning or 3D reconstruction. For 3D iterative techniques, the attenuation coefficients can be utilized directly within the reconstruction model. Most typically, the attenuation coefficients are calculated by the forward projection of (preprocessed) transmission images. However, forward projection into 4D parameter (fully 3D data) space is a time consuming operation which might take considerably more time than the reconstruction itself, as in the case of FORE+2D/2.5D reconstruction approaches. For this reason, simplified approaches are often used in routine clinical use, such as rebinning of raw emission data without attenuation correction and applying (2D) attenuation correction afterwards. This substantially speeds-up the attenuation correction calculations, since only non-oblique attenuation factors are needed, but introduces additional errors into the reconstruction process. As part of the development of Direct Fourier Reconstruction with Fourier Reprojection (3D_FRP) [12], we have implemented fast Fourier based forward projector (FoProj) allowing for very fast calculation of fully 3D attenuation data and making proper treatment of the attenuation information within the fully 3D reconstruction process more practical.

In this work, we compare performance of the 3D and 2.5D iterative Row Action Maximum Likelihood Algorithm (RAMLA) [3,13] using blobs on the efficient spatial (BCC) grid. We also evaluate the impact of using attenuation correction information in the reconstruction algorithm. 3D PET data obtained from a clinical C-PET (ADAC UGM) whole body scanner are used in our study.

II. Methods

A. Reconstruction Algorithms

The row action maximum likelihood algorithm (RAMLA) [13] was developed as a faster alternative to the maximum likelihood expectation maximization (ML-EM) algorithm for maximizing the Poisson likelihood in PET. In RAMLA, the reconstructed image is updated for each projection line (row of the system matrix) in a controlled way using a relaxation parameter. The $(k+1)$'th update step, where $k \geq 0$, produces an image represented by a set of basis function coefficients $\{ c_j^{(k+1)} \}_{j=1}^{J}$ using the formula

$$c_j^{(k+1)} \;=\; c_j^{(k)} \;+\; \lambda_k c_j^{(k)} \left(\frac{g_{i_k}}{\langle a_{i_k}, c^{(k)} \rangle} - 1 \right) a_{i_k,j} \;, \qquad (1)$$

where $i_k = [k(modI) + 1]$, g_{i_k} and $\langle a_{i_k}, c^{(k)} \rangle$ represent the measured data and forward projection for the i_k'th line, respectively, and λ_k is the relaxation parameter (including normalization factor) fulfilling the condition $\lambda_k a_{i_k,j} \leq 1$ for every i_k, j [13]. The data are accessed using a special ordering scheme [14] to ensure that the sequential projection lines are as orthogonal as possible, thus considerably speeding-up the rate of convergence. RAMLA achieves stable performance and relative independence on the starting point via an appropriately chosen relaxation parameter, controlling the amount of updates/corrections in each iteration step.

In the studies reported in this paper we used a 3D implementation of RAMLA using blobs - modified Kaiser-Bessel basis functions of second order [4] located on the standard cubic (voxel) grid and on the efficient BCC grid [10] of various grid step sizes. To study the improvement of the true 3D reconstruction over the (pseudo 3D) reconstruction from rebinned data we employed 2.5D RAMLA [6], which is currently our best reconstruction technique for rebinned PET data.

We applied 3D RAMLA and 2.5D RAMLA (after FORE) to phantom and patient datasets. To determine optimal parameters for each reconstruction algorithm for a given activity distribution, the data were reconstructed and analyzed for a range of parameters and blob sizes (FWHM) by varying the blob radius a (2-3, relative to voxel size of 4mm), blob shape parameter α (chosen as described by Matej and Lewitt [1, 10]), grid spacing g for the BCC grid (1.8-2.26, relative to voxel size), and relaxation parameter λ (0.001-0.1). In most cases, performing more than one iteration of RAMLA did not significantly improve image quality. The representative reconstruction times for a set of comparable reconstruction parameters ($a = 2.5$, $\alpha = 8.63$, $g = 2.00$, 1 iteration, data: 128 radial bins, 64 slices, 96 views, 7 tils, image: 144x144x64 with 4x4x4mm^3 voxels) obtained on single processor Sparc Ultra 10 (440MHz) were: 3D RAMLA (regular grid) 35:20 (min:sec), 3D RAMLA (BCC grid) 6:45, 2.5D RAMLA 1:56 (including 1min for FORE).

B. Attenuation Effects

We studied various ways of utilization of attenuation information: reconstructions from data precorrected for attenuation in the fully 3D data space (4DAC), date corrected in the rebinned data space (2DAC), and reconstructions using attenuation information within the system model (sysAC). The attenuation coefficients were obtained by forward projection of the transmission images. Transmission images were reconstructed from a ^{137}Cs single-photon source transmission data, rescaled to 511-keV, and segmented [15]. The transmission data were rebinned using the single-slice rebinning algorithm (SSRB) [16] and corrected for emission contamination [17].

Forward projection was calculated using fast Fourier based projector (FoProj) [12]. The computation time for complete 4D attenuation coefficient/correction data (image:144x144x64, data:128x64x96x7) was 0.8 min, as compared to 3.7 min for the forward projection based on the Siddon algorithm [18]. Although, both times are clinically reasonable for this image size, the ratio between them increases approximately proportionally to the im-

age size increase (based on the computation complexity of $O(N^3 logN)$ for FoProj versus $O(N^4)$ for Siddon). Additional substantial speed-up of the FoProj algorithm can be obtained by using (off-the-shelf) FFT processor boards.

C. Torso Phantom Studies

The IEC phantom distribution recently adopted by the NEMA Coincidence Imaging Task Force for the measurement of image quality [19] was used to mimic patient imaging of the torso. The distribution consists of a torso phantom, containing hot and cold spheres in a warm background. The hot spheres have diameters of 1.0, 1.3, 1.7, and 2.2 cm; the cold spheres have diameters of 2.8 and 3.7 cm. A 5 cm diameter lung-like insert is also placed in the center of the phantom to provide a nonuniform attenuation distribution. The background was filled with ^{18}F at an activity concentration typical of what is seen in patient FDG studies (250MBq in 70kg, or 3.6kBq/cc). The hot spheres were filled with an activity concentration of 30 kBq/cc, for a "tumor":background activity ratio of 8:1. Scan durations of 3, 6, and 12 min were selected to generate a wide range of count densities. The ADAC UGM C-PET scanner with a maximum axial acceptance angle of $\pm 15°$, sorted into 7 tilt angles, was used.

To quantitate the performance of the algorithms, regions of interest (ROIs) with diameters equal to the physical inner diameter of each sphere were drawn on the slice through the centers of the spheres. Twelve ROIs of the same sizes as those for the spheres were drawn throughout the background in the central slice, as well as in slices ± 8 mm and ± 20 mm away. The coefficient of variation of the means in these 60 background ROIs was determined for each sphere size as a measure of the background variability. The hot sphere contrast recovery coefficient (CRC_{hot}) was calculated as

$$CRC_{hot} = (C_{hot}/C_{bkg} - 1)/(a_{hot}/a_{bkg} - 1) \qquad (2)$$

where C_{hot} and C_{bkg} are the average of the counts measured in the hot sphere ROI and the average of the counts in all 60 background ROIs, respectively, and a_{hot}/a_{bkg} is the ratio of the activities in the hot sphere and background (8 in this study). The cold sphere contrast recovery coefficient (CRC_{cold}) was calculated as

$$CRC_{cold} = (1 - C_{cold}/C_{bkg}) \qquad (3)$$

where C_{cold} is the average of the counts measured in the cold sphere ROI.

D. Whole-body Patient Studies

Several clinical whole-body patient studies were acquired after injection of 250MBq/70kg of [^{18}F]-FDG on the ADAC UGM C-PET scanner. The five-frame studies covered 70 cm axially. The acquisition followed an interleaved emission (6 min) / transmission (1.5 min) protocol.

III. Results and Discussion

Figure 1 shows for the IEC phantom data a plot of contrast vs. background variability for the 6-min scan for 3D RAMLA_BCC using various blob, grid and λ parameters. The plots for each feature size form approximately a single curve. The points representing results for 3D RAMLA using a regular cubic grid (solid symbols) and optimal parameters (based on our previous studies) lie on the same curves, showing that the two methods provide similar contrast versus noise tradeoff for an appropriate choice of parameters. At the same time, RAMLA_BCC provide about 5.2-times shorter reconstruction time. The comparable quality of the two methods was also confirmed by the visual observation of the reconstructed phantom and patient images.

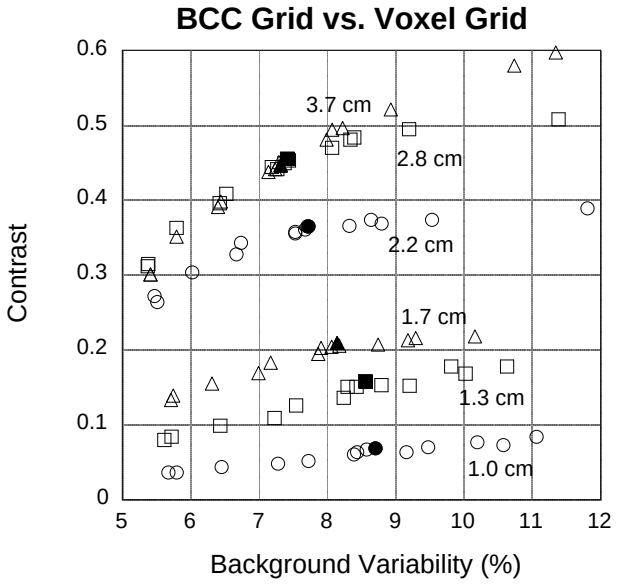

Fig. 1. Plots for the 6 spheres (4 smallest are hot, 2 largest are cold) for 6-min scan. The open symbols are for various blob and grid parameters (a:α:g = 2:3.6:2.26, 3:9.5:2.26, 2.5:8.63:2.00, 3:13.06:1.8) and various λ for 3D RAMLA using BCC grid. The closed symbols are for one representative reconstruction by slower version of RAMLA (a:α = 3.0:12.95) using standard cubic grid. We can obtain comparable contrast/variability performance with RAMLA_BCC for an appropriate choice of blob/grid parameters as with slower version of 3D RAMLA, but in about 1/5 the reconstruction time.

Figure 2 shows example of the study using IEC phantom comparing 2.5D reconstruction with 2D attenuation precorrection done after FORE to the 3D RAMLA (BCC) with system attenuation correction within the model. The first approach represents a simplification of the theory, but as can be seen in the left image, it still provides reasonable images and is often employed in the routine clinical use because of its low computational demands. The improvement due to proper use of the attenuation information in the fully 3D reconstruction algorithm is demonstrated by the increase of the background uniformity and the increase of the contrast of the features.

Figure 3 shows similar comparison for the whole-body patient study. On the left is coronal image of 2.5D RAMLA with pre-correction for attenuation after FORE using 2D attenuation correction factors. On the right is the corresponding slice for 3D RAMLA with system-modeling of attenuation effects using 4D attenuation correction factors generated using FoProj. It is evident that the fully 3D

Fig. 2. 6-min IEC phantom study reconstructed using 2.5D RAMLA with 2DAC (left side) and 3D RAMLA with sysAC (right side). It can be seen that the background is more uniform with 3D RAMLA and system-modeling of attenuation effects.

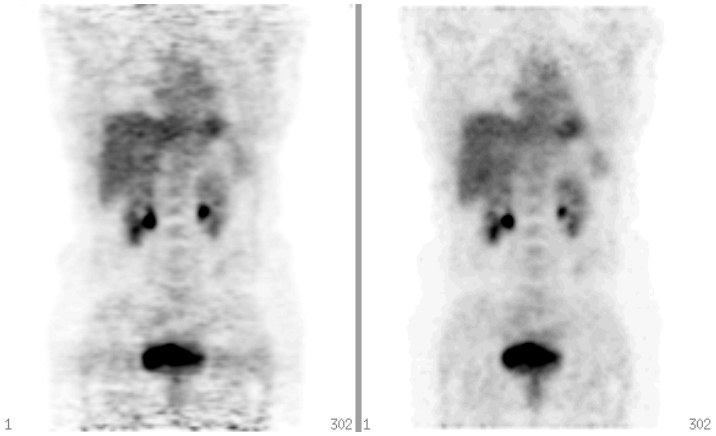

Fig. 3. Patient whole-body study (coronal images) reconstructed using 2.5D RAMLA with 2DAC (left side) and 3D RAMLA with sysAC (right side). It can be clearly seen that 3D RAMLA provides more uniform and less noisy reconstruction. The bladder streak artifacts seen throughout the slices of the 2.5D/2DAC reconstruction are completely absent in the 3D/sysAC reconstruction.

reconstruction together with the system modeling of the attenuation provides a definite improvement of the image quality. This is demonstrated by a combination of increased background uniformity, decreased noise and suppression of the bladder artifacts.

Examples shown in Figures 2 and 3 represent two ways to utilize attenuation information. The first - 2DAC after FORE - is oversimplified but is a very fast approach, while the second - system modeling with 4DAC - is more theoretically sound but is significantly slower. Note, that due to the developments discussed in this paper, even the second approach is now becoming feasible for the clinical use. There are several intermediate possibilities between these two extremes, such as using 4DAC+FORE+2D iterative reconstruction (OS-EM) which is in use at other clinical sites [11]. Our observations suggest that both the system modeling of attenuation and the use of a fully 3D reconstruction algorithm (rather than rebinning) lead to improvements in image quality. We are currently investigating the influence of individual steps on the reconstruction quality of the PET images in a more rigorous way employing measures of contrast and noise, as represented by the study in Figure 1. The results will be used to guide the data processing and image reconstruction protocols for the whole body patient studies.

References

[1] S. Matej and R. M. Lewitt, "Practical considerations for 3D image reconstruction using spherically-symmetric volume elements," *IEEE Trans. Med. Imaging*, vol. 15, no. 1, pp. 68–78, 1996.

[2] S. Matej, G. T. Herman, T. K. Narayan, S. S. Furuie, R. M. Lewitt, and P. E. Kinahan, "Evaluation of task-oriented performance of several fully 3D PET reconstruction algorithms," *Phys. Med. Biol.*, vol. 39, no. 3, pp. 355–367, 1994.

[3] S. Matej and J. A. Browne, "Performance of a fast maximum likelihood algorithm for fully 3D PET reconstruction," in *Series Computational Imaging and Vision: Three-Dimensional Image Reconstruction in Radiology and Nuclear Medicine*, P. Grangeat and J.-L. Amans, Eds., pp. 297–316. Kluwer Academic Publishers, Dordrecht, The Netherlands, 1996.

[4] R. M. Lewitt, "Multidimensional digital image representations using generalized Kaiser-Bessel window functions," *J. Opt. Soc. Am. A*, vol. 7, no. 10, pp. 1834–1846, 1990.

[5] M. Defrise, P. E. Kinahan, D. W. Townsend, C. Michel, M. Sibomana, and D. F. Newport, "Exact and approximate rebinning algorithms for 3D PET data," *IEEE Trans. Med. Imaging*, vol. 16, no. 2, pp. 145–158, 1997.

[6] T. Obi, S. Matej, R. M. Lewitt, and G. T. Herman, "2.5D simultaneous multislice reconstruction by series expansion methods from Fourier-rebinned PET data," *IEEE Trans. Med. Imaging*, vol. 19, no. 5, pp. 474–484, 2000.

[7] M. E. Daube-Witherspoon, S. Matej, J. S. Karp, and R. M. Lewitt, "Application of the row action maximum likelihood algorithm with spherical basis functions to clinical PET imaging," *IEEE Trans. Nucl. Sci.*, vol. 48, no. 1, pp. 24–30, 2001.

[8] S. Matej, J. S. Karp, R. M. Lewitt, and A. J. Becher, "Performance of the Fourier rebinning algorithm for PET with large acceptance angles," *Phys. Med. Biol.*, vol. 43, no. 4, pp. 787–795, 1998.

[9] J. S. Karp, A. J. Becher, S. Matej, and P. E. Kinahan, "Data processing and image reconstruction methods for the HEAD PENN-PET scanner," *IEEE Trans. Nucl. Sci.*, vol. 45, no. 3, pp. 1144–1151, 1998.

[10] S. Matej and R. M. Lewitt, "Efficient 3D grids for image reconstruction using spherically-symmetric volume elements," *IEEE Trans. Nucl. Sci.*, vol. 42, no. 4, pp. 1361–1370, 1995.

[11] C. Comtat, P. E. Kinahan, M. Defrise, C. Michel, and D. W. Townsend, "Fast reconstruction of 3D PET data with accurate statistical modeling," *IEEE Trans. Nucl. Sci.*, vol. 45, no. 4, Part 2, pp. 1083–1089, 1998.

[12] S. Matej, "3D-FRP: Direct Fourier reconstruction with Fourier reprojection for fully 3D PET," in *Proceedings of the 2000 IEEE Nuclear Science Symposium and Medical Imaging Conference. CDROM, IEEE572*. Lyon, France, October 15-20, 2000, To be published.

[13] J. A. Browne and A. R. De Pierro, "A row-action alternative to the EM algorithm for maximizing likelihoods in emission tomography," *IEEE Trans. Med. Imaging*, vol. 15, no. 5, pp. 687–699, 1996.

[14] G. T. Herman and L. B. Meyer, "Algebraic reconstruction techniques can be made computationally efficient," *IEEE Trans. Med. Imaging*, vol. 12, no. 3, pp. 600–609, 1993.

[15] R. J. Smith, J. S. Karp, G. Muehllehner, E. Gualtieri, and F. Bénard, "Singles transmission scans performed post-injection for quantitative whole body PET imaging," *IEEE Trans. Nucl. Sci.*, vol. 44, no. 3, pp. 1329–1335, 1997.

[16] M. E. Daube-Witherspoon and G. Muehllehner, "Treatment of axial data in three-dimensional PET," *J. Nucl. Med.*, vol. 28, pp. 1717–1724, 1987.

[17] J. S. Karp, G. Muehllehner, H. Qu, and X. H. Yan, "Singles transmission in volume-imaging PET with a ^{137}Cs source," *Phys. Med. Biol.*, vol. 40, pp. 929–944, 1995.

[18] R. L. Siddon, "Fast calculation of the exact radiological path for a three-dimensional CT array," *Med. Phys.*, vol. 12, no. 2, pp. 252–255, 1985.

[19] J. S. Karp, R. J. Smith, G. Muehllehner, M. E. Daube-Witherspoon, and H. Hines, "Image quality measurement for evaluation of PET scanner performance (abstract)," *J. Nucl. Med.*, vol. 39, no. 5, pp. 133P–134P, 1998.